metals

MDPI

Article

Effect of Solution Heat Treatment by Induction on UNS S31803 Duplex Stainless Steel Joints Welded with the Autogenous TIG Process

Paula Munier Ferreira [1], Elaine Cristina Pereira [1], Flávia Wagner Pinheiro [1], Sergio Neves Monteiro [2] and Afonso R. G. Azevedo [3,*]

1 LAMAV-Advanced Materials Laboratory, University of the Northern Rio de Janeiro, Av. Alberto Lamego, 2000, Campos dos Goytacazes 28013-602, Brazil
2 Materials Engineering Section (SE/8), IME-Materials Science Program, Military Engineering Institute, Praça Gen. Tibúrcio, 80, Urca, Rio de Janeiro 22290-270, Brazil
3 LECIV-Civil Engineering Laboratory, UENF-State, University of the Northern Rio de Janeiro, Av. Alberto Lamego, 2000, Campos dos Goytacazes 28013-602, Brazil
* Correspondence: afonso.garcez91@gmail.com

Abstract: In the oil and gas industry, the manufacture of equipment using materials that resist aggressive media is one of the greatest challenges. UNS S31803 duplex stainless steel is widely used for this purpose owing to its good combination of mechanical and corrosion resistance. The objective of this work was to evaluate the effect of induction solution heat treatment using autogenous TIG welding on UNS S31803 DSS sheets. Sheet samples were subjected to two different treatment parameters for a duration of 10 s and at temperatures of 1050 and 1150 °C. The results obtained with the treatments were compared with those of the as-welded condition, which was the reference condition. Quantitative and qualitative analyses of the samples were carried out, in addition to microstructural characterization using confocal microscopy and a corrosion resistance study as per ASTM G48 standard. We observed that the best results were obtained with a treatment of 10 s at 1150 °C, which was able to eliminate chromium nitrides and re-establish the proper balance of the ferrite and austenite phases. In addition, the treatment was able to reduce hardness and provide welds free of cracks and discontinuities, also presenting a low corrosion rate.

Keywords: duplex stainless steel; welding; corrosion; solution heat treatment

check for updates

Citation: Ferreira, P.M.; Pereira, E.C.; Pinheiro, F.W.; Monteiro, S.N.; Azevedo, A.R.G. Effect of Solution Heat Treatment by Induction on UNS S31803 Duplex Stainless Steel Joints Welded with the Autogenous TIG Process. *Metals* **2022**, *12*, 1450. https://doi.org/10.3390/met12091450

Academic Editors: Aihan Feng, Zhenbo Zhang and Hao Wang

Received: 29 July 2022
Accepted: 23 August 2022
Published: 30 August 2022

Publisher's Note: MDPI stays neutral with regard to jurisdictional claims in published maps and institutional affiliations.

Copyright: © 2022 by the authors. Licensee MDPI, Basel, Switzerland. This article is an open access article distributed under the terms and conditions of the Creative Commons Attribution (CC BY) license (https://creativecommons.org/licenses/by/4.0/).

1. Introduction

The dual-phase microstructure of duplex stainless steels (DSSs) consists of equally balanced volumetric fractions of ferrite and austenite. This steel is commonly used in the manufacture of equipment in the oil and gas industry due to its combination of favorable characteristics, such as mechanical and corrosion resistance. However, the service behavior of this material depends on its microstructure, which is strongly influenced by thermal processes, such as welding, which can lead to microstructural changes [1,2].

UNS S31803 is a DSS that combines these two properties. The use of this material in aggressive media has been increasingly explored in the oil industry, and its use has occurred in numerous areas, especially in the production of flexible pipelines. However, this DSS, when subjected to high temperatures, can have its microstructural characteristics altered, and these changes can lead to the loss of important properties. Excess ferrite and undesirable precipitates might cause catastrophic deterioration of properties, especially corrosion resistance and toughness [3].

Most applications of DSSs require some welding process, and for this reason, their weldability has been the subject of extensive investigation [4]. Although modern DSSs are designed to have excellent weldability, being able to be welded by most processes, it is

necessary to adapt the welding procedure due to the fact that dual-phase microstructures are sensitive to the imposed conditions [4,5]. For example, when welding a DSS with high heat input, ferrite can be converted to CrN and Cr_2N, while austenite does not undergo the same process [6]. Thus, some precautions need to be taken regarding the parameters and welding procedures performed, aiming at the preservation of mechanical properties and corrosion resistance [4]. Therefore, practices such as carrying out the process of welding in narrow ranges of welding energy and performing temperature control, for example, must be adopted. However, this might not be always possible or sufficient; therefore, it is necessary to carry out post-weld heat treatments (PWHTs), which aim to reduce the residual stresses generated due to solidification in order to avoid the propagation of welding cracks and, mainly, to solubilize the undesirable precipitates in order to re-establish the equilibrium of the ferrite and austenite phases [7]. A literature review [8,9] showed that there is a strong relationship between the PWHT parameters, microstructure, and pitting corrosion behavior of welded joints. The main types of heat treatment associated with welding operations are annealing, normalizing, tempering, solubilization, quenching, preheating, postheating, and stress relief.

Currently, most studies [10,11] have applied heat treatments to dissolve the secondary phases and improve the ferrite/austenite balance, and for this, the solution heat treatment is applied. This consists of a treatment that makes a dissolution, in the solid state, of elements that were previously precipitated, followed by cooling fast enough to allow these elements to retain in the matrix. Its purpose is to leave the material in the best condition for application, dissolving most of the precipitates formed during the solidification process.

There are many types of postweld heat treatments, of which induction heat treatment is one of the most energy-saving and high-efficiency methods. As pointed out by some authors [12], the high heating rate and short retention time of induction heating can increase austenitization superheating as well as the austenite nucleation rate. This is beneficial for obtaining uniform and fine austenite grain and improving the strength and toughness of subsequent cooling transition products [12]. In addition, unlike traditional heat treatment methods, induction heating can be performed in situ without the need to remove the parts and localize the heat by altering the voltage distribution at a given spot on the component. In addition, by designing the shape and size of the induction coil, the method can produce parts with complex structures [13]. Zhang et al. investigated the influence of induction and treatment postweld heat treatments on the corrosion properties of SAF 2205; they found that induction heating creates a significant thermal gradient and different corrosion resistances along the weld bead thickness.

The literature indicates [14–16] that there is a strong relationship between the heat treatment parameters (temperature and time) as well as the morphology, phase fraction, and dissolution of precipitates on the material's microstructure. Thus, the objective of this research was to characterize and evaluate the effects of different parameters of induction solubilization heat treatment on the microstructure of the base metal (BM), the fusion zone (FZ), and the heat-affected zone (HAZ) of DSS type UNS S31803.

2. Materials and Methods

Samples of UNS S31803 DSS, commercially known as SAF 2205, were used on sheets with a thickness of 2.5 mm. This DSS is generally used in the manufacture of flexible pipes. Table 1 shows the chemical composition of the UNS S31803 sheets.

Table 1. Composition of UNS S31803 (wt %) [17].

Element	C	Mn	Si	Cr	Ni	P	S	Mo
Content	0.03	1.37	0.47	21.0–23.0	4.5–6.5	0.03	0.01	2.5–3.5

The sheets were welded by the automatic TIG process, with a pulsed direct current, direct polarity (DC-), and without the addition of metal, thus configuring an autogenous

process. Three samples were prepared. After the welding procedure, two of them were subjected to induction solution heat treatment, dissolving precipitates that were formed during the solidification process in the welding. The treatments were carried out at temperatures of 1050 and 1150 °C, for a duration of 10 s. Cooling was conducted naturally, in air, to room temperature (RT). The two samples were compared with the condition without heat treatment, named "reference condition" or "as-welded condition".

The welded samples were cut in order to evaluate their microstructure along three regions: edge, 1/4 region, and 1/2 region, as shown in Figure 1. The length and width of the samples were 25 and 7 mm, respectively.

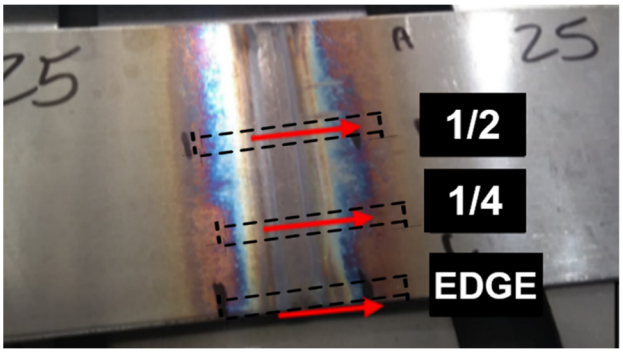

Figure 1. Indication of the cut regions in the welded sheet.

The samples were then subjected to metallographic preparation, passing through the steps of embedding, sanding, polishing, and two different etching methods, for comparison purposes. The initial method of etching was performed by immersing the samples in Behara I solution (0.3 g of $K_2S_2O_3$ + 10 mL of $Na_2S_2O_3 \cdot 5H_2O$ in 100 mL of distilled water) for a period of 60 s. This etching revealed only the ferrite and austenite phases. The second method performed was the electrolytic etching, with the immersion of the samples in a 10% oxalic acid solution, current of 3 A, voltage of 3 V, and etching time ranging from 6 to 20 s. This etching revealed, in addition to the ferrite and austenite phases, the presence of chromium nitrides (CrN e Cr_2N).

Confocal (model Olympus OLS400, Shinjuku, Tóquio, Japão) and optic (model Olympus BX51M, Shinjuku, Tóquio, Japão) microscopes were used in order to perform the qualitative and quantitative microstructural characterization of the samples. The characterization of the microstructure was carried out to evaluate not only the microstructure of the base metal (BM), the heat affected zone (HAZ), and the fusion zone (FZ) but also the possible precipitates, such as nitrides and carbides. In addition, it allowed quantitative analysis.

2.1. Quantitative Analysis of Phases

The quantitative analysis allowed the quantification of ferrite present in the samples. This quantification was performed using two different methods for comparison purposes. The first one was the manual method of counting points, specified in the ASTM E562-11 [18] standard, superimposing a mesh of 100 points on each image of interest. We captured 20 images per sample, 10 from the HAZ and 10 from the FZ. The images, in this case, were obtained using an Olympus OLS400 confocal microscope, (model Olympus OLS400, Shinjuku, Tóquio, Japão) with a magnification of 1075×. This quantification method was applied to samples with microstructures obtained after electrolytic etching with 10% oxalic acid, which revealed the ferrite and austenite phases and the chromium nitrides. The second method was applied through a BX51M microscope (Olympus, Shinjuku, Tóquio, Japão), which works with Stream Essentials software (1 St. version; USA) for capturing images and quantification. For this, Behara I etching was used. The count was automatically performed through the difference between the tonality of the phases because this etching makes the austenite light (white) and the ferrite dark (black/grey). The recording of the images, in this case, was performed using an Olympus BX51M microscope (Olympus,

Shinjuku, Tóquio, Japão) at 500× magnification. We captured 30 images per sample, 15 from the HAZ and 15 from the FZ.

The quantification performed by the two methods provided the percentage of ferrite in each of the recorded images. From this, the average was calculated for each region of each sample. Thus, 30 averages were obtained with each method. The values found by the manual method were statistically compared with the values obtained with the automatic method. This comparison was performed using Student's *t*-test to verify whether the two quantification methods were equivalent. A significance level of 5% was considered. In addition, Student's *t*-test also evidenced the variance, which measures statistical dispersion, i.e., it shows how far the data are from the expected value (average). From this, it was possible to determine which of the two methods presented the smallest dispersion.

2.2. Bending Test

Two bending tests were applied for each condition. The test was carried out in a P10ST hydraulic press (SOLOTEST, São Paulo, Brazil), and for each tape, the test was repeated toward the top and root of the weld. The ASME IX [19] standard was followed. After the bending test, the liquid penetrant test was performed in order to assess whether there were cracks and discontinuities in the weld resulting from the bending constraint.

2.3. Hardness Test

For hardness measurements, an automatic Tukon 250 microhardness tester (TUKON, Berlin, Germany) was used, applying the Vickers hardness method with a load of 500 g (HV 0.5), during a period of 10 s. Six hardness test analyses were performed, and symmetry in the weld structure was considered, with two indentations within each zone to be analyzed. It was performed passing through the BM, HAZ, and FZ on one sample of each welded condition. The markings performed in this test were made according to the hardness profile shown in Figure 2.

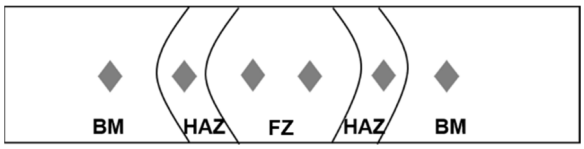

Figure 2. Vickers hardness profile used.

2.4. Corrosion Test

Corrosion tests were performed using ferric chloride, according to ASTM G48 [20]–method A. It was necessary to remove the samples used in the metallographic test from each condition to obtain specimens to perform the corrosion tests. Thus, 9 samples were obtained to be tested. The three regions of the weld, of each welding condition, containing FZ, HAZ, and part of the adjacent BM, were subjected to the test. The corrosion rate was calculated according to the equations of NACE RP 0775 [21].

3. Results and Discussion

3.1. Qualitative Analysis

Figure 3 shows the microstructure found in the BM of UNS S31803, where the distribution of elongated austenite lamellae (lighter phase) immersed in a ferritic matrix (darker phase) in the lamination direction can be observed. This is the characteristic structure of this type of material. It is possible to perceive an apparently equivalent distribution between these phases. The microstructure observed is consistent with that described by Freitas et al. [22] for laminated DSS.

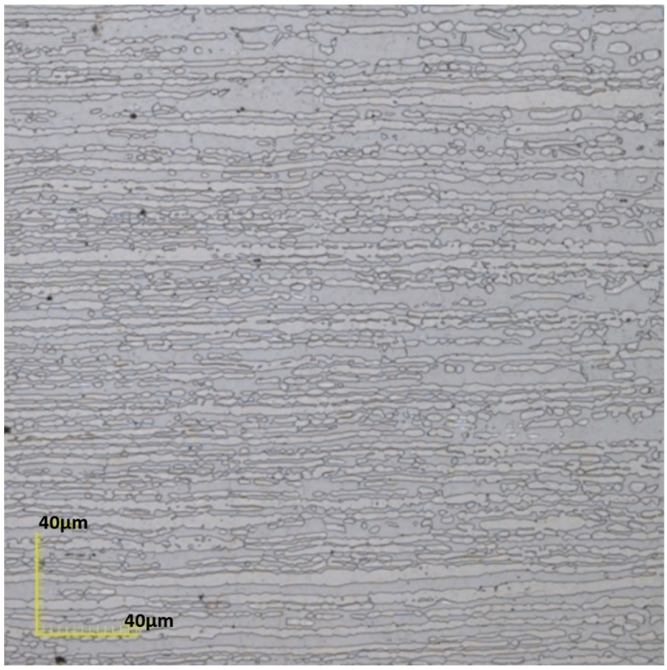

Figure 3. Representative microstructure of the BM. Electrolytic etching with 10% oxalic acid. Confocal microscopy (model Olympus OLS400, Shinjuku, Tóquio, Japão), 1075× magnification.

Figures 4 and 5 represent the microstructure found after the welding process (reference condition) in the FZ and HAZ, respectively. It is possible to perceive a morphological alteration of the present phases. The initially elongated grains of ferrite and austenite, observed in the BM, were altered after the thermal cycle imposed by the welding process. In addition, it is possible to observe in the images in Figures 4 and 5 the different morphologies of austenite: grain boundary austenite (GBA), Widmanstatten austenite (WA), and intragranular austenite (IGA), which is consistent with the microstructure found in similar work [23].

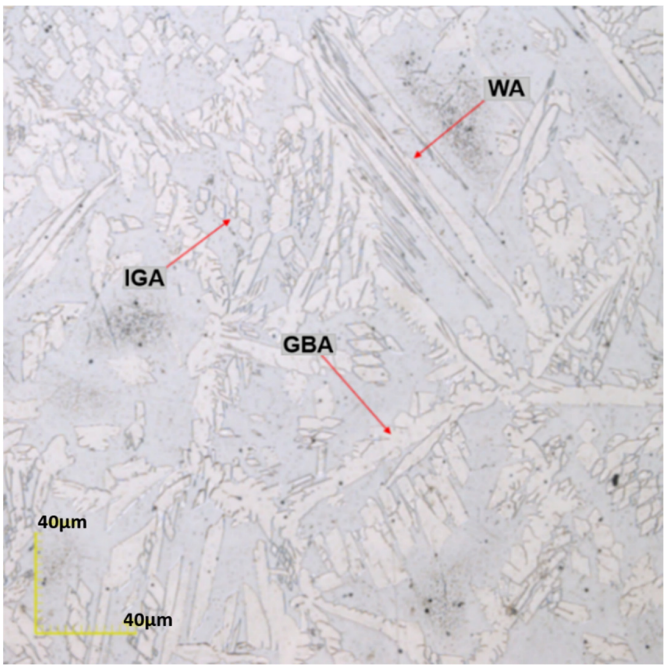

Figure 4. Representative microstructure found in the FZ. Electrolytic etching with 10% oxalic acid. Confocal microscopy (model Olympus OLS400, Shinjuku, Tóquio, Japão), 1075× magnification.

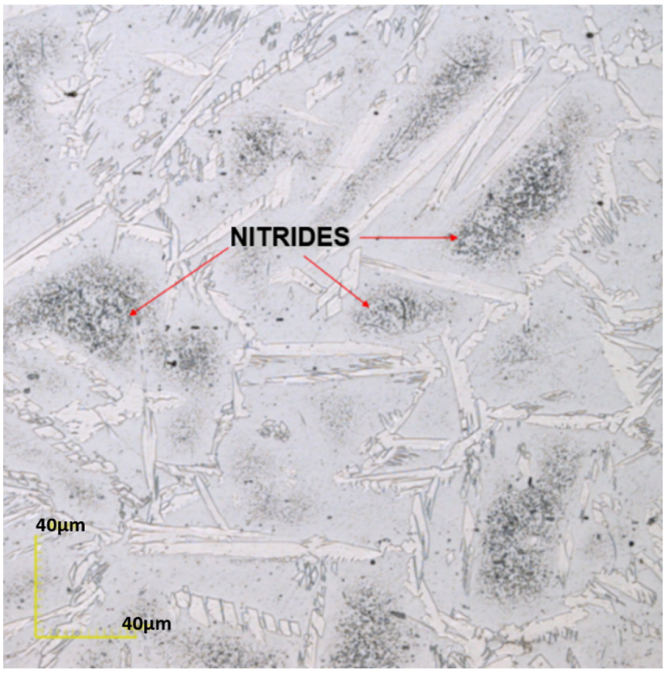

Figure 5. Representative microstructure found in the HAZ. Electrolytic etching with 10% oxalic acid. Confocal microscopy (model Olympus OLS400, Shinjuku, Tóquio, Japão), 1075× magnification.

In addition, it is possible to visually notice the imbalance in the proportion of the phases, as cited by several authors [5,24,25]. As a result, an excessive ferrite content and precipitation of chromium nitrides were observed in the HAZ, as described. In the FZ, there were a lower fraction of ferrite and, consequently, a lower amount of chromium nitrides compared with the HAZ.

In general, the microstructure characteristics seen in the BM, HAZ, and FZ of the reference condition (as welded) were similar to those observed in the other heat-treatment conditions applied in this work.

3.2. Microstructural Characterization

3.2.1. As Welded Condition

The as-welded condition was the reference condition, which did not receive any heat treatment. The welding energy used was 2.81 KJ/mm. Figure 6 shows the microstructure observed in the FZ of the as-welded condition sample.

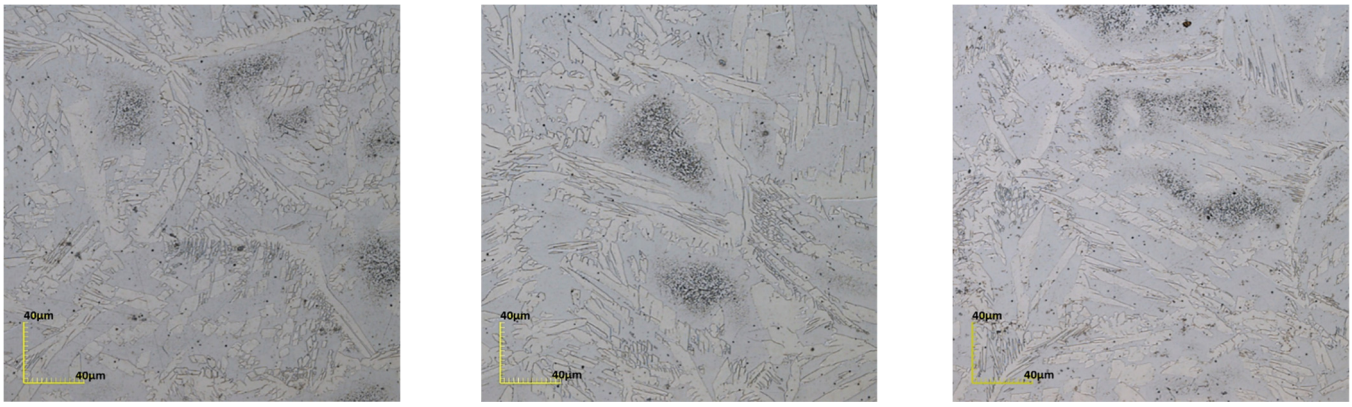

(**a**) (**b**) (**c**)

Figure 6. Microstructure observed in the FZ of the as-welded condition sample: (**a**) edge; (**b**) 1/4 region; (**c**) 1/2 region.

It is possible to observe a typical microstructure of a DSS welded with low welding energy, presenting a ferritic and austenite matrix with a morphology of larger grains and without preferential direction, in addition to the presence of chromium nitrides in the ferritic matrix, as described [12]. This was seen both at the edge and in the 1/4 and 1/2 regions. A large amount of chromium nitrides was present in the microstructure in all regions of the sheet, both in the FZ and HAZ. However, there was a greater amount of precipitation of these nitrides in the HAZ, owing to the high amount of ferrite in this region, which was due to the low heat input and welding without filler metal (autogenous). The microstructure found in the HAZ can be seen in Figure 7.

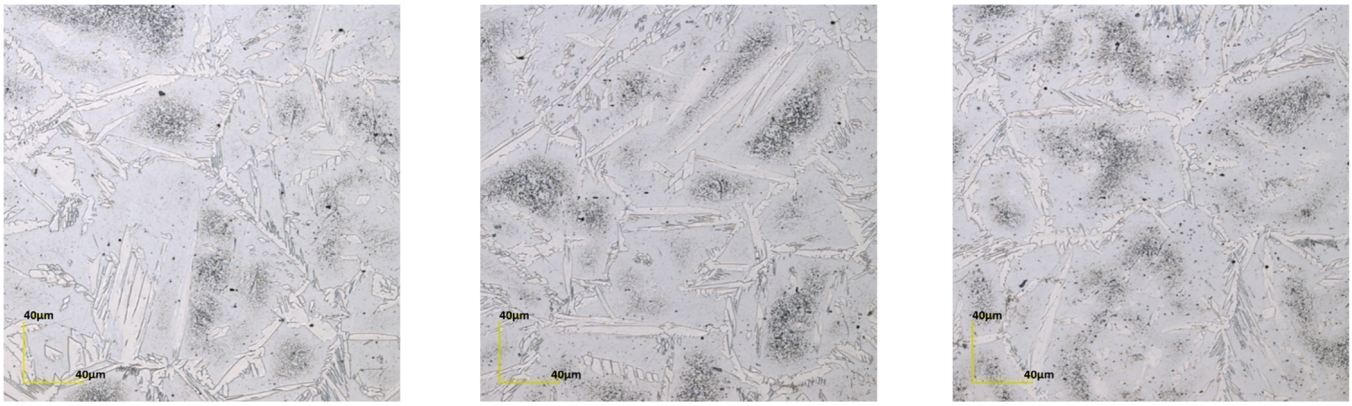

(**a**) (**b**) (**c**)

Figure 7. Microstructure observed in the HAZ of the as welded condition sample: (**a**) edge; (**b**) 1/4 region; (**c**) 1/2 region.

No intermetallic precipitates were identified in the microstructure other than chromium nitride (Cr_2N).

3.2.2. Solution Heat Treatment for 10 s at 1050 °C

The microstructure found in the FZ and HAZ of the sample treated at 1050 °C for 10 s is shown in Figures 8 and 9, respectively.

(**a**) (**b**) (**c**)

Figure 8. Microstructure observed in the FZ of the sample subjected to postwelding solution heat treatment for 10 s at 1050 °C: (**a**) edge; (**b**) 1/4 region; (**c**) 1/2 region.

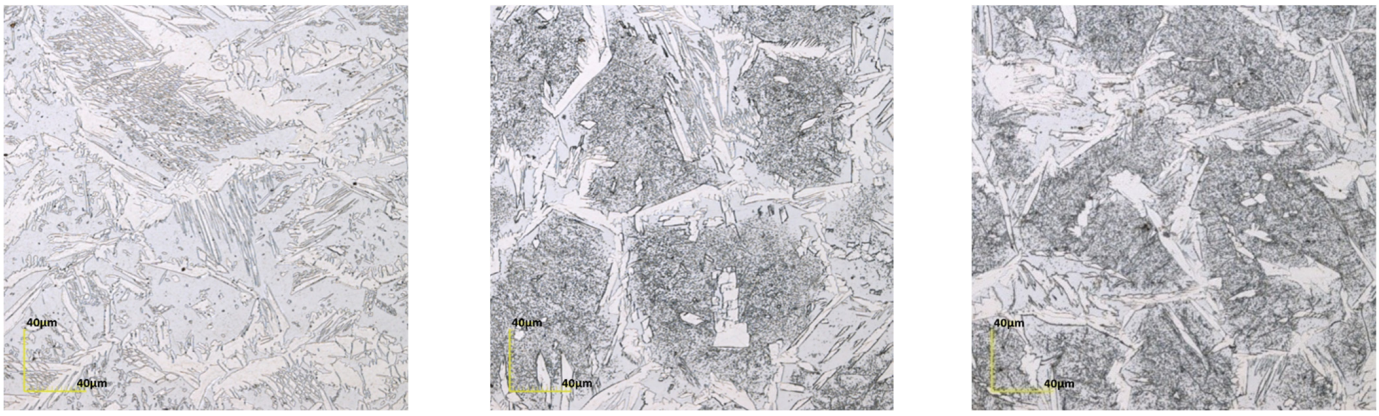

(**a**) (**b**) (**c**)

Figure 9. Microstructure observed in the HAZ of the sample subjected to postwelding solution heat treatment for 10 s at 1050 °C: (**a**) edge; (**b**) 1/4 region; (**c**) 1/2 region.

In the FZ, the edge region showed high austenite content and microstructure with no nitrides. However, the 1/4 and 1/2 regions showed a high fraction of chromium nitrides in a greater amount than in the welded condition, with ferrite and austenite contents apparently close to equilibrium.

In the HAZ, the absence of nitrides was also observed in the edge region, but with a proportion of ferrite to austenite close to equilibrium. The 1/4 and 1/2 regions showed high volumetric fractions of chromium nitrides in a considerably higher amount than in the welded condition. Furthermore, in these regions, the ferrite content was considerably higher. The presence of chromium nitrides in the microstructure, even after postwelding heat treatment, could be attributed to the low temperature of the solubilization combined with insufficient retention time for the dissolution of these precipitates [26].

3.2.3. Solution Heat Treatment for 10 s at 1150 °C

The microstructure observed in the FZ and HAZ of the sample treated at 1150 °C for 10 s is shown in Figures 10 and 11, respectively.

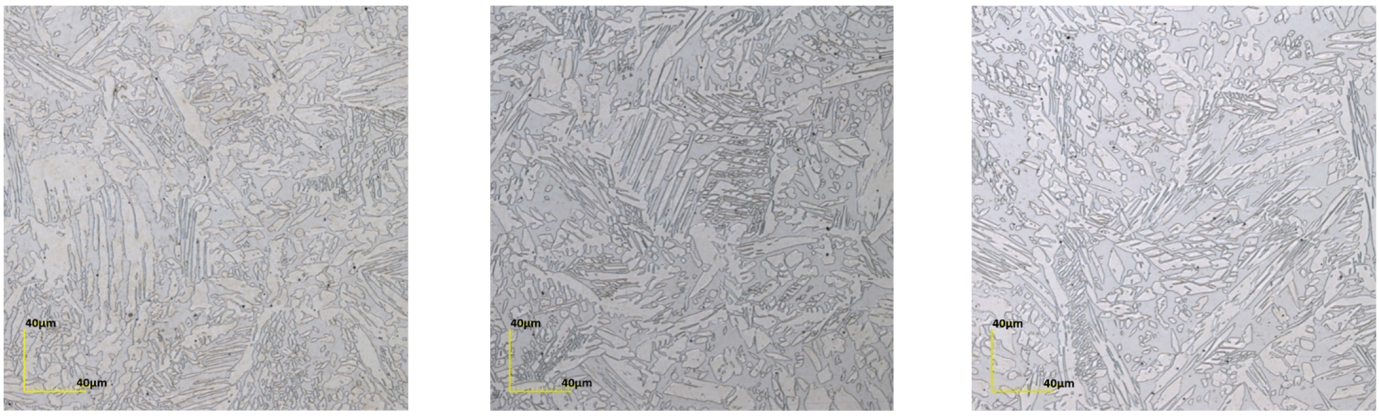

(**a**) (**b**) (**c**)

Figure 10. Microstructure observed in the FZ of the sample subjected to postwelding solution heat treatment for 10 s at 1150 °C: (**a**) edge; (**b**) 1/4 region; (**c**) 1/2 region.

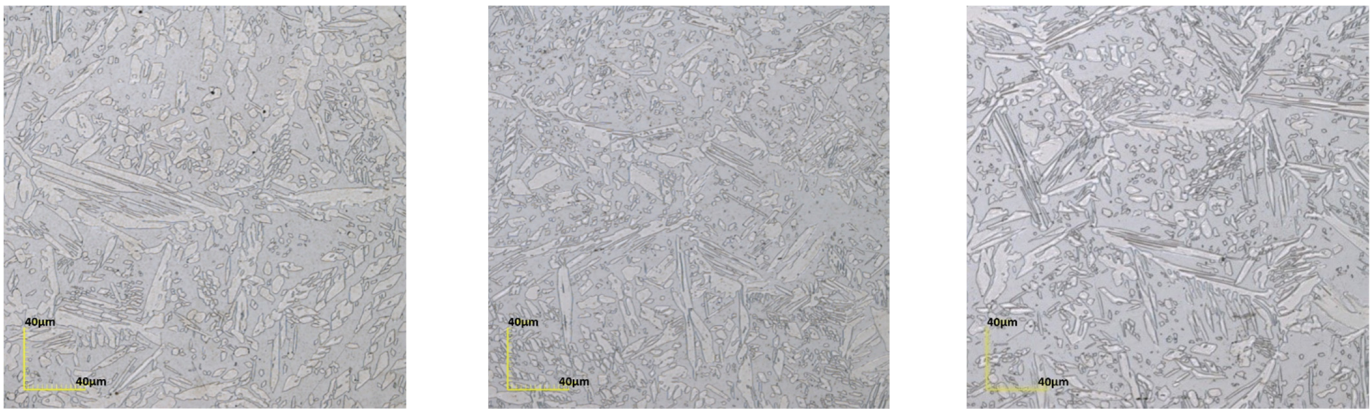

(**a**) (**b**) (**c**)

Figure 11. Microstructure observed in the HAZ of the sample subjected to postwelding solution heat treatment for 10 s at 1150 °C: (**a**) edge; (**b**) 1/4 region; (**c**) 1/2 region.

In this condition, the edge, as well as the 1/4 and 1/2 regions, did not present nitrides in a significant amount in their microstructure, either in the FZ or HAZ. Thus, we found that the chromium nitrides were significantly solubilized in the ferritic matrix after the induction solution heat treatment in the different weld regions analyzed. Thus, we affirmed that PWHT promoted the dissolution of the nitrides [26].

PWHT also caused an increase in austenite content, and this behavior was the same for edge, 1/4, and 1/2 regions. In the FZ, the austenite content became higher than that of ferrite but maintained a proportion considered acceptable. In the HAZ, there was a balance between the proportions of ferrite and austenite. We also noted the presence of different austenite morphologies: WA, IGA, and GBA.

3.3. Methods Used

3.3.1. Manual Method

In general, all samples presented ferrite percentage values within the recommended range of 30% to 70%. The exceptions were the entire HAZ of the welded condition, which presented a phase imbalance, as expected, and the edge of the weld zone of the sample treated at 1050 °C for 10 s, which presented values very close to the lower limit of 30% (namely, 28%).

The reference condition showed high levels of ferrite in the HAZ in all regions of the weld (reaching 75%), corroborating what was qualitatively observed in the microstructural characterization; while in the FZ, the percentages were close to equilibrium.

The treatment at 1050 °C for 10 s showed unbalanced ferrite levels in both the WZ and HAZ. In the HAZ, with the exception of the edge, high ferrite content was found (reaching 70% in the 1/2 region). In the FZ, a low ferrite content was observed in the edge region (28%), which explains the absence of chromium nitrides in this region; in the 1/2 region, a higher content (58%) was observed. The trend of an increasing percentage of ferrite was identified from the edge to the middle of the weld. Therefore, we found that the heat treatment applied in this condition was not able to re-establish the balance between the phases.

With the treatment at 1150 °C for 10 s, ferrite contents considered acceptable in all regions were identified. In the HAZ, values very close to equilibrium (from 49% to 51%) were obtained; in the FZ, lower percentages of ferrite were obtained but within the satisfactory limit. Thus, the heat treatment applied to this condition was able to re-establish the balance between the phases along the joint.

3.3.2. Automatic Method

As for the manual method, all samples showed ferrite levels within the recommended range of 30% to 70%. The exceptions were the entire HAZ of the welded condition, which presented a phase imbalance, as expected, and the 1/2 region of the HAZ of the sample treated at 1050 °C for 10 s. Despite this, the values remained very close to the upper limit of 70%.

The reference condition showed high levels of ferrite in the HAZ in all regions of the weld; in the HAZ, the percentages were close to equilibrium.

With the treatment at 1050 °C for 10 s, in the HAZ, with the exception of the edge, a high ferrite content was found (reaching 72% in the 1/4 region). In the FZ, a lower ferrite content was observed in the edge region (34%), while the 1/4 and 1/2 regions maintained values close to equilibrium. The trend of an increasing percentage of ferrite was identified from the edge to the middle of the weld.

In the treatment at 1150 °C for 10 s, all percentage values of ferrite and austenite were close to equilibrium.

3.3.3. Statistical Analysis for Comparison of Methods: Student's *t*-Test

After 30 tests, 15 hypotheses were accepted at a significance level of 0.05 (α = 5%). Thus, the manual and automatic methods for phase quantification were equivalent for 50% of the comparisons, with a confidence level of 95%.

The test also showed that the variance of the quantification of the automatic method, in general, was smaller than that of the manual method. Of 30 tests performed for comparison, the variance of the automatic method was significantly lower than that of the manual method in 77% of cases. Although the methods were equivalent, the low dispersion between the values obtained in the automatic method showed greater precision, as well as the accuracy and reliability of data extracted from the images.

3.4. Bending Test

After evaluation, we found that all specimens subjected to the bending and penetrating liquid test obtained results considered satisfactory according to the ASME IX criterion [19], which defines that the test is acceptable if there are no cracks and discontinuities greater than 3.2 mm. None of the welded conditions presented cracking and/or opening in the weld.

3.5. Hardness Test

The hardness results ranged from 247 to 303 HV, with a mean value of 269.58 ± 12.07 HV overall. According to NACE Standard MR0103-2016 [27], for welded DSSs, the average hardness should not exceed 310 HV, and no individual reading should exceed 320 HV. We found that all the values found were within the acceptable limit. Table 2 shows the mean of the results for each sample.

Table 2. Average hardness value for each sample.

Sample	Hardness
A- welded condition	276.78 ± 6.44
10 s at 1050 °C	278.61 ± 11.45
10 s at 1150 °C	262.72 ± 9.43

It can be seen that the as-welded condition and treatment for 10 s at 1050 °C presented the highest hardness values, showing very close values. This was possibly due to the greater precipitation of chromium nitrides in these samples. In addition, these were the samples that presented higher ferrite contents, and an increase in the amount of ferrite increased the hardness of the DSS because ferrite has a microstructure with greater hardness [3].

The hardness results showed that the change in the investigated heat treatment parameters did not cause significant effects. Therefore, all welded conditions were satisfactory.

3.6. Corrosion Resistance

Table 3 shows the results found for the corrosion rate under each of the conditions.

Table 3. Average corrosion rate of each sample.

Corrosion Rate	As-Welded	10 s at 1050 °C	10 s at 1150 °C
(mm/a)	2.2379	7.0744	0.1485
(g/m^2d)	45.7234	152.8710	3.1920

It can be seen that the treatment at 1050 °C for 10 s showed the highest corrosion rate, even higher than the as-welded condition. This findings confirms the results previously seen because this was the sample that presented the highest amount of chromium nitrides, in addition to a large proportion of ferrite. The high corrosion rate was attributed to the high number of nitrides in the ferritic matrix. These results showed that PWHT was not effective because the corrosion rate values found in this group were close to or even worse than those in the condition without PWHT. In addition, we observed that the highest incidence of corrosion occurred in the 1/2 region of the weld.

The lowest corrosion rate was found for the sample treated at 1150 °C for 10 s, which presented a microstructure free of chromium nitrides and with proportions of ferrite and austenite within the expected limit. This confirmed the results previously seen in the microstructure, with the absence of nitrides and a close-to-equilibrium phase ratio.

4. Conclusions

For the sample treated at 1050 °C for 10 s, the postweld heat treatment (PWHT) was considered partially efficient, being effective at the edge but not effective in the other regions. Compared with the welded condition, it presented similar hardness values but was not able to significantly reduce the ferrite content in all regions. Only the edge microstructure showed the solubilization of chromium nitrides, while the 1/4 and 1/2 regions showed high proportions of this precipitate. The corrosion rate in this condition was higher, with a value about three times higher than in the welded condition, confirming that the PWHT under these parameters was not efficient.

For the sample treated at 1150 °C for 10 s, the PWHT was considered efficient. The microstructure along the entire weld (edge, 1/4, and 1/2 regions) became free of nitrides, with ferrite and austenite contents close to equilibrium and considered acceptable. Hardness was also reduced compared with that in the welded condition. Thus, the microstructure after heat treatment resulted in a low rate of pitting corrosion.

The automatic method of phase quantification showed less dispersion of results compared with those of the manual method. In addition, the need for considerably less time for analysis is considered adequate.

We found that postweld solution heat treatment, in general, was able to reduce the hardness and provide acceptable welds, with no cracks or discontinuities, according to the results of the bending test. The results of the corrosion test confirmed what was seen in the microstructural analyses: the corrosion rate was higher for higher ferrite contents and increased precipitation of chromium nitrides.

Author Contributions: Conceptualization, P.M.F. and A.R.G.A.; Formal analysis, E.C.P.; Methodology, F.W.P. and A.R.G.A.; Project administration, S.N.M. and A.R.G.A. All authors have read and agreed to the published version of the manuscript.

Funding: This research was funded by the State University of the Northern Fluminense (UENF), partially financed by CAPES (Coordenação de Aperfeiçoamento de Pessoal de Nível Superior—Brazil) and provided additional financial by CNPq (Coordenação Nacional de Pesquisa) Code 309428/2020-3. The participation of A.R.G.A. was sponsored by FAPERJ through the research fellowships proc.no: E-26/210.150/2019, E-26/211.194/2021, E-26/211.293/2021, E-26/201.310/2021 and by CNPq through the research fellowship PQ2 307592/2021-9.

Institutional Review Board Statement: Not applicable.

Informed Consent Statement: Not applicable.

Data Availability Statement: Not applicable.

Conflicts of Interest: The authors declare no conflict of interest.

References

1. Sim, B.M.; Hong, T.S.; Hanim, M.A.A.; Tchan, E.J.N.; Talari, M.K. The Influence of Post Weld Heat Treatment Precipitation on Duplex Stainless Steels Weld Overlay towards Pitting Corrosion. *Materials* **2019**, *12*, 3285. [CrossRef] [PubMed]
2. Shamanth, V.; Ravishankar, K.S.; Hemanth, K. Duplex Stainless Steels: Effect of Reversion Heat Treatment. In *Stainless Steels and Alloys*; IntechOpen: London, UK, 2019. [CrossRef]
3. de Souza, D.D.B.G.; Vilarinho, L.O. Influence of Present Phases in Corrosion and Mechanical Behavior of UNS S31803 Duplex Stainless Steel Welded by Conventional Short Circuit MIG/MAG Process. *J. Mater. Res. Technol.* **2020**, *9*, 11244–11254. [CrossRef]
4. Elsaady, M.A.; Khalifa, W.; Nabil, M.A.; El-Mahallawi, I.S. Effect of Prolonged Temperature Exposure on Pitting Corrosion of Duplex Stainless Steel Weld Joints. *Ain Shams Eng. J.* **2018**, *9*, 1407–1415. [CrossRef]
5. Sasikumar, C.; Sundaresan, R.; Medona, C.M.; Ramakrishnan, A. Corrosion Study on AA-TIG Welding of Duplex Stainless Steel. *Mater. Today Proc.* **2021**, *45*, 3383–3385. [CrossRef]
6. Devendranath Ramkumar, K.; Chandrasekhar, A.; Srivastava, A.; Preyas, H.; Chandra, S.; Dev, S.; Arivazhagan, N. Effects of Filler Metals on the Segregation, Mechanical Properties and Hot Corrosion Behaviour of Pulsed Current Gas Tungsten Arc Welded Super-Austenitic Stainless Steel. *J. Manuf. Processes* **2016**, *24*, 46–61. [CrossRef]
7. Selvabharathi, R. Effect of Post Weld Heat Treatment and TiAlSiN Coating on the Tensile Strength of Autogenous Plasma Arc Welding of Duplex/Super Austenitic Stainless Steels. *J. Manuf. Processes* **2019**, *38*, 135–147. [CrossRef]
8. Kumar, R.; Varma, A.; Kumar, Y.R.; Neelakantan, S.; Jain, J. Enhancement of Mechanical Properties through Modified Post-Weld Heat Treatment Processes of T91 and Super304H Dissimilar Welded Joint. *J. Manuf. Processes* **2022**, *78*, 59–70. [CrossRef]
9. Kainth, M.; Singh, M.; Singh, A. Effect of Filler Metal Combination and Post Weld Heat Treatment on Pitting Corrosion and Impact Toughness of GTA Welded AISI 410 SS Joints. *Mater. Today Proc.* **2022**, *56*, 3035–3041. [CrossRef]
10. Mampuya, M.B.; Umba, M.C.; Mutombo, K.; Olubambi, P.A. Effect of Heat Treatment on the Microstructure of Duplex Stainless Steel 2205. *Mater. Today Proc.* **2021**, *38*, 1107–1112. [CrossRef]
11. Zhang, D.; Wen, P.; Yin, B.; Liu, A. Temperature Evolution, Phase Ratio and Corrosion Resistance of Duplex Stainless Steels Treated by Laser Surface Heat Treatment. *J. Manuf. Processes* **2021**, *62*, 99–107. [CrossRef]
12. Zhang, W.; Zhao, G.; Fu, Q. Study on the Effects and Mechanisms of Induction Heat Treatment Cycles on Toughness of High Frequency Welded Pipe Welds. *Mater. Sci. Eng. A* **2018**, *736*, 276–287. [CrossRef]
13. Shen, H.; Lin, J.; Zhou, Z.; Liu, B. Effect of Induction Heat Treatment on Residual Stress Distribution of Components Fabricated by Wire Arc Additive Manufacturing. *J. Manuf. Processes* **2022**, *75*, 331–345. [CrossRef]
14. Köse, C.; Topal, C. Effect of Heat Input and Post-Weld Heat Treatment on Surface, Texture, Microstructure, and Mechanical Properties of Dissimilar Laser Beam Welded AISI 2507 Super Duplex to AISI 904L Super Austenitic Stainless Steels. *J. Manuf. Processes* **2022**, *73*, 861–894. [CrossRef]
15. Chaudhari, A.N.; Dixit, K.; Bhatia, G.S.; Singh, B.; Singhal, P.; Saxena, K.K. Welding Behaviour of Duplex Stainless Steel AISI 2205: A Review. *Mater. Today Proc.* **2019**, *18*, 2731–2737. [CrossRef]
16. Zhang, Z.; Jing, H.; Xu, L.; Han, Y.; Zhao, L.; Lv, X. Effect of Post-Weld Heat Treatment on Microstructure Evolution and Pitting Corrosion Resistance of Electron Beam-Welded Duplex Stainless Steel. *Corros. Sci.* **2018**, *141*, 30–45. [CrossRef]
17. Wu, X.; Yang, Y.; Sun, Y.; Liu, Y.; Li, J.; Jiang, Y. The Temperature-Dependent Pitting and Repassivation Behaviors of UNS S31803 Duplex Stainless Steel in Chloride Solutions. *Corros. Sci.* **2019**, *149*, 29–36. [CrossRef]
18. *ASTM E562*; Standard Test Method for Determining Volume Fraction by Systematic Manual Point Count. ASTM International: New York, NY, USA, 2019.
19. The American Society of Mechanical Engineers. *ASME Section IX: Qualification Standard for Welding and Brazing Procedures, Welders, Brazers, and Welding and Brazing Operators*; The American Society of Mechanical Engineers: New York, NY, USA, 2010.
20. *ASTM G48–11*; Standard Test Methods for Pitting and Crevice Corrosion Resistance of Stainless Steels and Related Alloys by Use of Ferric Chloride Solution. ASTM International: New York, NY, USA, 2015.
21. *NACE Standard RP 0775*; Preparation, Installation, Analysis and Interpretation of Corrosion Coupons in Oilfield Operations. NACE: New York, NY, USA, 2005.
22. Freitas, B.J.M.; Rodrigues, L.C.M.; Claros, C.A.E.; Botta, W.J.; Koga, G.Y.; Bolfarini, C. Ferritic-Induced High-Alloyed Stainless Steel Produced by Laser Powder Bed Fusion (L-PBF) of 2205 Duplex Stainless Steel: Role of Microstructure, Corrosion, and Wear Resistance. *J. Alloy. Compd.* **2022**, *918*, 165576. [CrossRef]
23. Mohammed, R.; Madhusudhan Reddy, G.; Srinivasa Rao, K. Effect of Welding Process on Microstructure, Mechanical and Pitting Corrosion Behaviour of 2205 Duplex Stainless Steel Welds. In Proceedings of the IOP Conference Series: Materials Science and Engineering; Institute of Physics Publishing: Bristol, UK, 2018; Volume 330. [CrossRef]

24. Gao, S.; Geng, S.; Jiang, P.; Mi, G.; Han, C.; Ren, L. Numerical Analysis of the Deformation Behavior of 2205 Duplex Stainless Steel TIG Weld Joint Based on the Microstructure and Micro-Mechanical Properties. *Mater. Sci. Eng. A* **2021**, *815*, 141303. [CrossRef]
25. Hou, Y.; Nakamori, Y.; Kadoi, K.; Inoue, H.; Baba, H. Initiation Mechanism of Pitting Corrosion in Weld Heat Affected Zone of Duplex Stainless Steel. *Corros. Sci.* **2022**, *201*, 110278. [CrossRef]
26. Tavares, S.S.M.; Pardal, J.M.; Noris, L.F.; Diniz, M.G. Microstructural Characterization and Non-Destructive Testing and of Welded Joints of Duplex Stainless Steel in Flexible Pipes. *J. Mater. Res. Technol.* **2021**, *15*, 3399–3408. [CrossRef]
27. *NACE MR0103*; Petroleum, Petrochemical and Natural Gas Industries—Metallic Materials Resistant to Sulfide Stress Cracking in Corrosive Petroleum Refining Environments. Springer: Geneva, Switzerland, 2016.